29. Jaccard, P. Nouvelles recherches sur la distribution florale. *Bull. Soc. Vaudoise Sci. Nat.* **44,** 223–270 (1908).

Acknowledgements We thank J. Bascompte, S. Cousins, S. Hubbell, R. Naisbit and P. Warren for useful comments. This work was funded by the Swiss National Science Foundation, the Novartis Foundation, and partly by the National Center of Competence in Research 'Plant Survival'.

Competing interests statement The authors declare that they have no competing financial interests.

Correspondence and requests for materials should be addressed to L.-F.B. (louis-felix.bersier@unine.ch).

Global organization of metabolic fluxes in the bacterium *Escherichia coli*

E. Almaas[1], B. Kovács[1,2], T. Vicsek[2], Z. N. Oltvai[3] & A.-L. Barabási[1]

[1]*Department of Physics, University of Notre Dame, Notre Dame, Indiana 46556, USA*
[2]*Biological Physics Department and Research Group of HAS, Eötvös University, H-1117 Budapest, Hungary*
[3]*Department of Pathology, Northwestern University, Chicago, Illinois 60611, USA*

Cellular metabolism, the integrated interconversion of thousands of metabolic substrates through enzyme-catalysed biochemical reactions, is the most investigated complex intracellular web of molecular interactions. Although the topological organization of individual reactions into metabolic networks is well understood[1–4], the principles that govern their global functional use under different growth conditions raise many unanswered questions[5–7]. By implementing a flux balance analysis[8–12] of the metabolism of *Escherichia coli* strain MG1655, here we show that network use is highly uneven. Whereas most metabolic reactions have low fluxes, the overall activity of the metabolism is dominated by several reactions with very high fluxes. *E. coli* responds to changes in growth conditions by reorganizing the rates of selected fluxes predominantly within this high-flux backbone. This behaviour probably represents a universal feature of metabolic activity in all cells, with potential implications for metabolic engineering.

To identify the interplay between the underlying topology[1–3] of the metabolic network of *E. coli* K12 MG1655 and its functional organization, we focus on the global features of potentially achievable flux states in this model organism with a fully sequenced and annotated genome[13,14]. In accordance with flux balance analysis (FBA)[8–12], we first identified the solution space (that is, all possible flux states under a given condition) by using constraints imposed by the conservation of mass and the stoichiometry of the reaction system for the reconstructed *E. coli* metabolic network[8–12]. Assuming that cellular metabolism is in a steady state and optimized for the maximal growth rate, FBA allows us to calculate the flux for each reaction using linear optimization[8–11], which provides a measure of the relative activity of each reaction.

As previously shown[8–10], the steady state and optimality approximations offer experimentally verifiable predictions on the flux states of the cell. Under any condition, however, there are also expected differences, some stemming from the fact that there are transient effects and that the growth rate is not always exactly optimal[12]. A marked feature of the obtained flux distribution is its overall inhomogeneity: reactions with fluxes spanning several orders of magnitude coexist under the same conditions. For example, under optimal growth conditions in a glutamate-rich culture, the dimensionless flux of the succinyl coenzyme A synthetase reaction is 0.185, whereas the flux of the aspartate oxidase reaction is four orders of magnitude smaller, with a value of 2.2×10^{-5} in dimensionless units (the flux vector is normalized to unity).

To characterize the coexistence of such widely different flux values, we plot the flux distribution for active (non-zero flux) reactions of *E. coli* grown in a glutamate- or succinate-rich substrate (Fig. 1a). The distribution is best-fitted with a power law with a small flux constant, indicating that the probability that a reaction has flux ν follows $P(\nu) \propto (\nu + \nu_0)^{-\alpha}$, where the constant is $\nu_0 = 0.0003$ and the flux exponent has the value $\alpha = 1.5$. The observed power law is also consistent with published experimental data. Indeed, the flux distribution obtained from the measured fluxes of the central metabolism of *E. coli*[15] is best-fitted with the power-law form (Fig. 1d). As the central metabolism is characterized by high fluxes, the small-flux saturation seen in Fig. 1a is absent from these data.

To examine whether the observed flux distribution is independent of the environmental conditions, we mimicked the influence of various growth conditions by randomly choosing 10%, 50% or 80% of the 96 potential substrates that *E. coli* can consume (the input substrates are listed in Supplementary Table S2). After optimizing the growth rate, we find that the power-law distribution of metabolic fluxes is independent of the external conditions (Fig. 1b). As the metabolic activity of *E. coli* frequently deviates from the optimal growth state under variable growth conditions[10,12], we inspected whether the wide flux distribution is also present in non-optimal

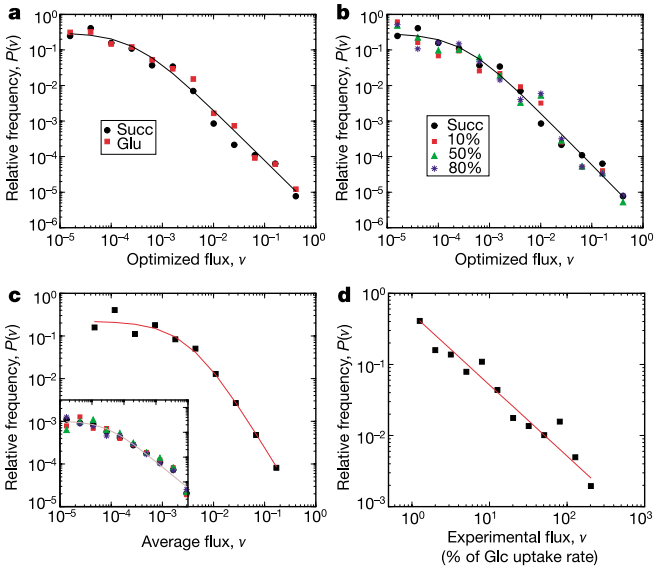

Figure 1 Characterizing the overall flux organization of the *E. coli* metabolic network. **a**, Flux distribution for optimized biomass production on succinate (black) and glutamate (red) substrates. Solid line corresponds to the power-law fit $P(\nu) \propto (\nu + \nu_0)^{-\alpha}$, with $\nu_0 = 0.0003$ and $\alpha = 1.5$. **b**, Flux distribution for optimized biomass on succinate (black) substrate with an additional 10% (red), 50% (green) and 80% (blue) randomly chosen subsets of the 96 input channels turned on. The flux distribution was averaged over 5,000 independent random choices of uptake metabolites. The resulting flux distribution can be fitted (solid line) by a power law with parameters $\nu_0 = 0.0004$ and $\alpha = 1.5$. **c**, Flux distribution from the non-optimized hit-and-run sampling method[16,17] of the *E. coli* solution space. The solid line is the best fit, with $\nu_0 = 0.003$ and $\alpha = 2$. Inset shows the flux distribution in four randomly chosen sample points. **d**, The distribution of experimentally determined fluxes (see ref. 15) from the central metabolism of *E. coli* shows power-law behaviour, with a best fit to $P(\nu) \propto \nu^{-\alpha}$ with $\alpha = 1$.

states. For this, we implemented a "hit-and-run" method[16,17] that randomly samples the full solution space, enabling us to calculate the flux for each reaction in 50,000 distinct non-optimal states.

Although the obtained average flux distribution is consistent in shape and flux ranges with those obtained by the optimal FBA, the flux exponent is slightly larger ($\alpha = 2$, Fig. 1c), and the quality of the scaling is slightly weaker. Notably, many individual non-optimal states (Fig. 1c, inset) are consistent with an exponent $\alpha = 1$, in accord with the experimental results (Fig. 1d) and supporting the prediction[10,12] that these organisms may not have achieved optimality. These findings imply that the observed flux distribution is a generic feature of flux conservation[18] on a scale-free network[19], as it is independent of the optimal or non-optimal nature of the growth rate or the growth conditions. The exponent, however, may depend on the organism's position in the solution space.

An exponentially decaying distribution (for example, a gaussian) would predict that under a given condition most reactions are characterized by comparable fluxes. By contrast, the identified power-law flux distribution suggests a highly uneven use: most reactions have small fluxes and coexist with a few reactions with very high flux values. Hence, the biochemical activity of the metabolism is dominated by several 'hot' reactions, which are embedded in a network of mostly small-flux reactions. The fact that the observed flux exponent α is less or equal to 2 implies that the first and higher moments of the flux distribution are not defined from a mathematical perspective (they diverge for an infinite system). The divergence of the average flux $\langle v \rangle$ (first moment) indicates that no flux value can be designated as characteristic for the system. Although $\langle v \rangle$ can be calculated numerically by averaging over the flux of all reactions, with $\langle v_g \rangle = 0.0171$ and $\langle v_s \rangle = 0.0173$ for glutamate and succinate uptakes, respectively, these values are by no means indicative of the overall activity of the metabolic reactions. Indeed, most reactions (86% for glutamate and 89% for succinate uptake) have a smaller flux than this average, and a few reactions have an activity that is orders of magnitude higher.

The observed flux distribution is compatible with two different potential local flux structures. A homogeneous local organization would imply that all reactions producing (consuming) a given metabolite have comparable fluxes; however, a more delocalized 'hot backbone' is expected if the local flux organization is heterogeneous, such that each metabolite has a dominant source (consuming) reaction (Supplementary Fig. S7). To distinguish between these two schemes for each metabolite i produced (consumed) by k reactions, we define the measure[20]

$$Y(k,i) = \sum_{j=1}^{k} \left(\frac{\hat{v}_{ij}}{\sum_{l=1}^{k} \hat{v}_{il}} \right) \qquad (1)$$

where $\hat{v}_{ij}$ is the mass carried by reaction j which produces (consumes) metabolite i. If all reactions producing (consuming) metabolite i have comparable $\hat{v}_{ij}$ values, $Y(k,i)$ scales as $1/k$. If, however, the activity of a single reaction dominates equation (1), we expect $Y(k,i) \propto 1$, in other words, $Y(k,i)$ is independent of k. For the *E. coli* metabolism optimized for succinate and glutamate uptake, we find

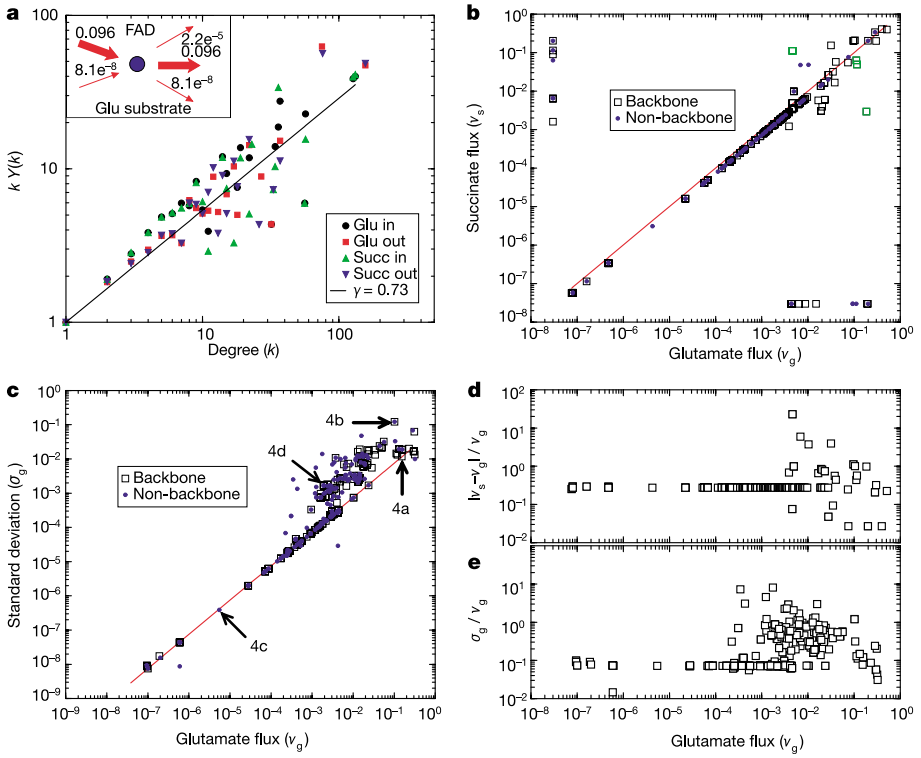

Figure 2 Characterizing the local inhomogeneity of the metabolic flux distribution. **a**, Measured $kY(k)$ shown as a function of k for incoming and outgoing reactions, averaged over all metabolites, indicates that $Y(k) \propto k^{-0.27}$, as the solid line has the slope $\gamma = 0.73$. Inset shows non-zero mass flows, $\hat{v}_{ij}$, producing (consuming) FAD on a glutamate-rich substrate. **b**, Change in the flux of individual reactions when switching from glutamate-rich (horizontal axis, v_g) to succinate-rich (vertical axis, v_s) conditions. Reactions with negligible flux changes follow the diagonal (solid line). Some reactions are turned off in only one of the conditions (shown close to the coordinate axes). Reactions belonging to the HFB (see Fig. 3) are indicated by black squares, the rest are indicated by blue dots. Reactions in which the direction of the flux is reversed are coloured green. **c**, Absolute value of glutamate flux (v_g) for 50% randomly chosen input channels (averaged over 5,000 realizations) plotted against the standard deviation of the same reaction. The red line, corresponding to $y = 0.075x$, is shown for reference. Numbers 4a–4d identify the reactions whose distribution is shown in Fig. 4. **d**, Relative flux change, $\Delta v = (|v_s - v_g|/v_g)$, as a function of v_g for the conditions shown in **b**. **e**, Relative fluctuation, σ_i/v_i, per reaction for the conditions shown in **c**, again emphasizing that large changes are limited to high-flux reactions.

that both the 'in' and 'out' degrees follow $Y(k,i) \propto k^{-0.27}$ (Fig. 2a), representing an intermediate behaviour between the two extreme cases. This indicates that the large-scale inhomogeneity observed in the overall flux distribution is also increasingly valid at the level of the individual metabolites: the more reactions that consume (produce) a given metabolite, the more likely it is that a single reaction carries most of the flux.

Such inhomogeneity is obvious, for example, for flavin adenine dinucleotide (FAD), whose production (consumption) is dominated by only one of the two (three) contributing reactions (Fig. 2a, inset), and the high-flux reactions are catalysed by succinate dehydrogenase complex, EC 1.3.5.1 (succinate dehydrogenase, EC 1.3.99.1). We find that $Y(k,i)$ scales in a similar fashion when *E. coli* is grown in rich Luria-Bertani medium or non-optimized configurations, indicating that the local inhomogeneity is not a unique feature of the optimized state or a specific growth condition but represents a generic property of the local flux distribution (see Supplementary Information).

The local flux inhomogeneity indicates that for most metabolites we can identify a single reaction that dominates its production (consumption). This observation can be turned into a simple algorithm, which for each metabolite systematically removes all reactions but the one providing the largest incoming (outgoing) flux contribution. The algorithm uncovers the 'high-flux backbone' (HFB) of the metabolism, a distinct structure of linked reactions that forms a giant component[21] with a star-like topology (Fig. 3 and Supplementary Fig. S12), including most metabolites produced under the given growth condition. Only a few pathways appear disconnected, indicating that although these pathways are part of the HFB, their end product is only the second-most important source for another HFB metabolite. Of note, groups of individual HFB reactions largely overlap with the traditional, biochemistry-based partitioning of cellular metabolism: for example, all metabolites of the citric acid cycle of *E. coli* are recovered, and so are a considerable fraction of other important pathways, such as those involved in histidine, murein and purine biosynthesis. The HFB

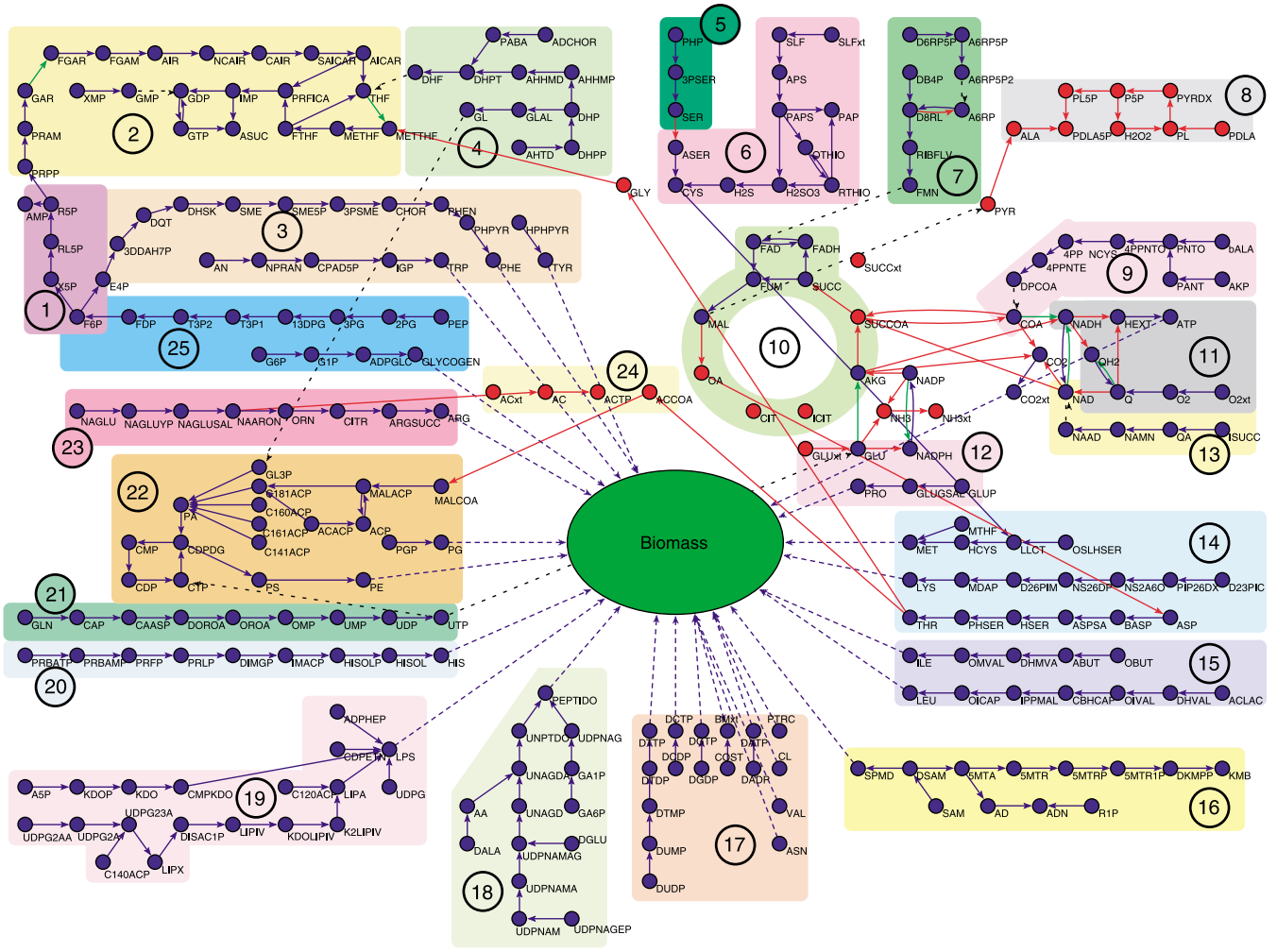

Figure 3 High-flux backbone for FBA-optimized metabolic network of *E. coli* on a glutamate-rich substrate (see Supplementary Fig. S12b for succinate-rich substrate). For any two metabolites (called for example, A and B) are connected with a directed link pointing from A to B only if the reaction with maximal flux consuming A is the reaction with maximal flux producing B. Shown are all metabolites that have at least one neighbour after completing this procedure. The background colours denote different known biochemical pathways. Metabolites (vertices) coloured blue have at least one neighbour in common in glutamate- and succinate-rich substrates, and those coloured red have none. Reactions (lines) are coloured blue if they are identical in glutamate- and succinate-rich substrates, green if a different reaction connects the same neighbour pair, and red if this is a new neighbour pair. Black dotted lines indicate where the disconnected pathways, for example, folate biosynthesis (4), would connect to the cluster through a link that is not part of the HFB. Thus, the red nodes and links highlight the predicted changes in the HFB when shifting *E. coli* from glutamate- to succinate-rich media. Dashed lines indicate links to the biomass growth reaction. Numbers identifying the various biochemical pathways are listed in the Supplementary Information.

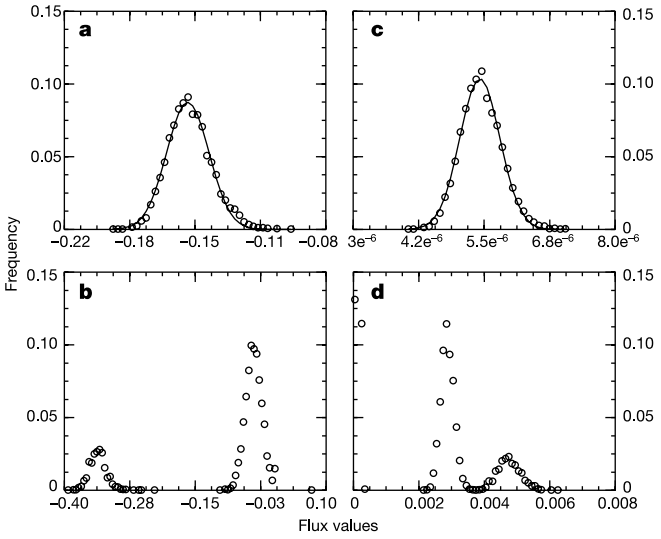

Figure 4 Effect of growth conditions on individual fluxes. Shown is the flux distribution for four select *E. coli* reactions in a 50% random environment (see Fig. 2c). **a**, Triosphosphate isomerase; **b**, carbon dioxide transport; **c**, NAD kinase; **d**, guanosine kinase. Reactions on the $\sigma \propto \nu$ curve have gaussian distributions (**a** and **c**); reactions off this curve have multimodal distributions (**b** and **d**), showing several discrete flux values under diverse conditions. Solid curves correspond to gaussians derived using the calculated ν and σ values of -0.15 and 0.012 (**a**) and $5.4e^{-6}$ and $3.9e^{-7}$ (**c**).

captures the subset of reactions that dominate the activity of the metabolism. As such, it offers a complementary approach to elementary flux mode analyses[22–24], which successfully capture the available modes of operation for smaller metabolic subnetworks.

As the flux of the individual metabolic reactions depends on the growth conditions, we need to inspect how sensitive the HFB is to changes in the environment. Unexpectedly, Fig. 2b, c, which records the relationship between the individual fluxes under succinate and glutamate uptake, indicates that only the reactions in the high-flux territory undergo noticeable flux changes, whereas the reactions in the intermediate- and low-flux regions remain virtually unaltered (a small shift can be observed, however, because there is a 41% increase in biomass production in glutamate-rich versus succinate-rich media). The observed flux changes correspond to two types of event. First, some pathways are turned off completely (type I reactions), having zero flux under one growth condition and high flux in the other. These reactions are shown as symbols along the horizontal and vertical axis in Fig. 2b. By contrast, other reactions remain active but show an orders-of-magnitude shift in flux under the two different growth conditions (type II reactions). Notably, with two exceptions these marked type II changes are limited to the HFB reactions. The same phenomenon is predicted when we inspect the transition from glucose to succinate uptake, or for transitions among various random uptake conditions (see Supplementary Information).

To test the generality of this finding, we mimicked the effect of various growth conditions by randomly choosing 50% of the potential input substrates, measuring in each input configuration the flux for each reaction. For each reaction, the average flux (ν) and the standard deviation (σ) around this average were determined by averaging over 5,000 random input conditions. For small fluxes, all reactions closely follow a straight line (corresponding to $\sigma \propto \nu$), supporting the above finding that the small fluxes remain essentially unaltered as the external conditions change (Fig. 2c). For the high-flux reactions, however, there are noticeable deviations from this line, indicating that there are considerable variations in flux from one external condition to the other (Fig. 2d, e). A closer inspection of the flux distribution shows that the reactions on the $\sigma \propto \nu$ curve all have a clear unimodal flux distribution (Fig. 4a, c), indicating that shifts in growth conditions lead to only small changes (within σ) of their flux values. By contrast, the reactions deviating from the $\sigma \propto \nu$ curve have a bi- or trimodal distribution, indicating that under different growth conditions they show several discrete and distinct flux values (Fig. 4b, d).

Therefore, Figs 2c–e, 3 and 4 offer valuable insights into how *E. coli* responds to changes in growth conditions: it activates or deactivates specific metabolic reactions among the HFB metabolites in new ways without altering the identity of the principal pathways that participate in the backbone. For example, switching from a glutamate to a succinate substrate turns off vitamin B6 biosynthesis (type I change), reconnects in other ways several metabolic substrates, such as those of the coenzyme A and NAD biosynthesis pathways as well as the respiration pathways, and modifies the use of the citric acid cycle (Supplementary Fig. S12). Apart from minor changes, the use of the other pathways remains unaltered. These reorganizations result in large, discrete changes in the fluxes of the HFB reactions.

The power-law distribution of metabolic fluxes in the *E. coli* metabolism indicates a highly uneven use of the underlying metabolic network topology. Although wide flux differences among various pathways are known from individual experiments[15,25–27], we find that they are part of a scale-invariant continuum, which follows a scaling law. The uneven flux use is present both at the global level (Fig. 1) and at the level of the individual metabolites (Fig. 2a). This observation allows us to uncover automatically the HFB of the metabolism and could provide insights into metabolic organization and regulation as well as offering valuable inputs for metabolic engineering.

The observation and theoretical prediction of a power-law load distribution in simple models (ref. 18 and Supplementary Information), coupled with the presence of a power law in both the optimal and non-optimal flux states, suggests that the metabolic flux organization is a direct consequence of the scale-free topology of the network[19]. As all organisms examined so far are characterized by a scale-free metabolic network topology[1], the observed scaling in the flux distribution is probably not limited to *E. coli*, but characterizes all organisms from eukaryotes to archaea. As FBA is available for an increasing number of prokaryotic and eukaryotic organisms, this prediction could be verified both experimentally and theoretically in the near future. Hence, the observed uneven local and global flux distribution seems to be rooted in the subtle, yet generic, interplay of the network's directed topology and flux balance, channelling the numerous small fluxes into high-flux pathways. The dependence of the scaling exponents characterizing the flux distributions on the nature of the optimization process, as well as the experimentally observed exponent, may be a benchmark for future structural and evolutionary models aiming to explain the origin, the organization and the modular structure[3,4,28,29] of cellular metabolism. □

Methods

Flux balance analysis

Starting from a stoichiometric matrix of the MG1655 strain[8,9] of *E. coli*, containing 537 metabolites and 739 reactions, the steady-state concentrations of all the metabolites satisfy:

$$\frac{\mathrm{d}}{\mathrm{d}t}[A_i] = \sum_j S_{ij}\nu_j = 0 \qquad (2)$$

where S_{ij} is the stoichiometric coefficient of metabolite A_i in reaction j and ν_j is the flux of reaction j. We use the convention that if metabolite A_i is a substrate (product) in reaction j, then $S_{ij} < 0$ ($S_{ij} > 0$), and we constrain all fluxes to be positive by dividing each reversible reaction into two 'forward' reactions with positive fluxes. Any vector of positive fluxes $\{\nu_j\}$ that satisfies equation (2) corresponds to a state of the metabolic network and, hence, a potential state of operation of the cell. We restrict our study to the subspace of solutions for which all components of ν satisfy the constraint $\nu_j > 0$ (ref. 8). We denote the mass carried

by reaction j producing (consuming) metabolite i by:

$$\hat{\nu_{ij}} = |S_{ij}|\nu_j$$

Random uptake conditions

We choose randomly X% (where $X = 10, 50$ or 80) of the 89 potential input substrates that *E. coli* consumes in addition to the minimal uptake basis. For each of the transport reactions, we set the uptake rate to 20 mmol per gram of dry weight per hour. As there are a very large number of possible combinations of the selected input substrates, we repeat this process 5,000 times and average over each realization.

The hit-and-run method

We select a set of basis vectors spanning the solution space using singular-value decomposition. Because the reaction fluxes must be positive, the 'bouncer' is constrained to the part of the solution space that intersects the positive orthant. We constrain the bouncer within a hypersphere of radius R_{max} and outside a hypersphere of radius $R_{min} < R_{max}$, where we find that the sampling results are independent of the choices of R_{min} and R_{max}. Starting from a random initial point inside the positive flux cone in a randomly chosen direction, the bouncer travels deterministically a distance d between sample points. Each sample point, corresponding to a solution vector where the components are the individual fluxes, is normalized by projection onto the unit sphere. After every bth bounce off the internal walls of the flux cone, the direction of the bouncer is randomized.

High-flux backbone

For each metabolite we keep only the reactions with the largest flux that produces and consumes the metabolite. Metabolites that are not produced (consumed) are discounted. Subsequently, a directed link is introduced between two metabolites A and B if (1) A is a substrate of the most active reaction producing B, and (2) B is a product of the maximal reaction consuming A. We consider only metabolites that are connected to at least one other metabolite after steps (1) and (2). For clarity, we remove P_i, PP_i and ADP. Further details and figures are provided in the Supplementary Information.

Received 29 August; accepted 12 December 2003; doi:10.1038/nature02289.

1. Jeong, H., Tombor, B., Albert, R., Oltvai, Z. N. & Barabási, A.-L. The large-scale organization of metabolic networks. *Nature* **407,** 651–654 (2000).
2. Wagner, A. & Fell, D. A. The small world inside large metabolic networks. *Proc. R. Soc. Lond. B* **268,** 1803–1810 (2001).
3. Ravasz, E., Somera, A. L., Mongru, D. A., Oltvai, Z. N. & Barabási, A.-L. Hierarchical organization of modularity in metabolic networks. *Science* **297,** 1551–1555 (2002).
4. Holme, P., Huss, M. & Jeong, H. Subnetwork hierarchies of biochemical pathways. *Bioinformatics* **19,** 532–538 (2003).
5. Savageau, M. A. *Biochemical Systems Analysis: a Study of Function and Design in Molecular Biology* (Addison-Wesley, Reading, MA, 1976).
6. Heinrich, R. & Schuster, S. *The Regulation of Cellular Systems* (Chapman & Hall, New York, 1996).
7. Goldbeter, A. *Biochemical Oscillations and Cellular Rhythms: the Molecular Bases of Periodic and Chaotic Behavior* (Cambridge Univ. Press, Cambridge, UK, 1996).
8. Edwards, J. S. & Palsson, B. O. The *Escherichia coli* MG1655 *in silico* metabolic genotype: its definition, characteristics, and capabilities. *Proc. Natl Acad. Sci. USA* **97,** 5528–5533 (2000).
9. Edwards, J. S., Ibarra, R. U. & Palsson, B. O. *In silico* predictions of *Escherichia coli* metabolic capabilities are consistent with experimental data. *Nature Biotechnol.* **19,** 125–130 (2001).
10. Ibarra, R. U., Edwards, J. S. & Palsson, B. O. *Escherichia coli* K-12 undergoes adaptive evolution to achieve *in silico* predicted optimal growth. *Nature* **420,** 186–189 (2002).
11. Edwards, J. S., Ramakrishna, R. & Palsson, B. O. Characterizing the metabolic phenotype: a phenotype phase plane analysis. *Biotechnol. Bioeng.* **77,** 27–36 (2002).
12. Segre, D., Vitkup, D. & Church, G. M. Analysis of optimality in natural and perturbed metabolic networks. *Proc. Natl Acad. Sci. USA* **99,** 15112–15117 (2002).
13. Blattner, F. R. *et al.* The complete genome sequence of *Escherichia coli* K-12. *Science* **277,** 1453–1474 (1997).
14. Gerdes, S. Y. *et al.* Experimental determination and system level analysis of essential genes in *Escherichia coli* MG1655. *J. Bacteriol.* **185,** 5673–5684 (2003).
15. Emmerling, M. *et al.* Metabolic flux responses to pyruvate kinase knockout in *Escherichia coli*. *J. Bacteriol.* **184,** 152–164 (2002).
16. Smith, R. L. Efficient Monte-Carlo procedures for generating points uniformly distributed over bounded regions. *Oper. Res.* **32,** 1296–1308 (1984).
17. Lovász, L. Hit-and-run mixes fast. *Math. Program.* **86,** 443–461 (1999).
18. Goh, K. I., Kahng, B. & Kim, D. Universal behavior of load distribution in scale-free networks. *Phys. Rev. Lett.* **87,** 278701 (2001).
19. Barabási, A.-L. & Albert, R. Emergence of scaling in random networks. *Science* **286,** 509–512 (1999).
20. Barthelemy, M., Gondran, B. & Guichard, E. Spatial structure of the Internet traffic. *Physica A* **319,** 633–642 (2003).
21. Ma, H. W. & Zeng, A. P. The connectivity structure, giant strong component and centrality of metabolic networks. *Bioinformatics* **19,** 1423–1430 (2003).
22. Dandekar, T., Schuster, S., Snel, B., Huynen, M. & Bork, P. Pathway alignment: application to the comparative analysis of glycolytic enzymes. *Biochem. J.* **343,** 115–124 (1999).
23. Schuster, S., Fell, D. A. & Dandekar, T. A general definition of metabolic pathways useful for systematic organization and analysis of complex metabolic networks. *Nature Biotechnol.* **18,** 326–332 (2000).
24. Stelling, J., Klamt, S., Bettenbrock, K., Schuster, S. & Gilles, E. D. Metabolic network structure determines key aspects of functionality and regulation. *Nature* **420,** 190–193 (2002).
25. Sauer, U. *et al.* Metabolic flux ratio analysis of genetic and environmental modulations of *Escherichia coli* central carbon metabolism. *J. Bacteriol.* **181,** 6679–6688 (1999).
26. Canonaco, F. *et al.* Metabolic flux response to phosphoglucose isomerase knock-out in *Escherichia coli* and impact of overexpression of the soluble transhydrogenase UdhA. *FEMS Microbiol. Lett.* **204,** 247–252 (2001).
27. Fischer, E. & Sauer, U. Metabolic flux profiling of *Escherichia coli* mutants in central carbon metabolism using GC-MS. *Eur. J. Biochem.* **270,** 880–891 (2003).
28. Hartwell, L. H., Hopfield, J. J., Leibler, S. & Murray, A. W. From molecular to modular cell biology. *Nature* **402,** C47–C52 (1999).
29. Wolf, D. M. & Arkin, A. P. Motifs, modules and games in bacteria. *Curr. Opin. Microbiol.* **6,** 125–134 (2003).

Supplementary Information accompanies the paper on **www.nature.com/nature**.

Acknowledgements We thank M. Bárász, J. Becker, E. Ravasz, A. Vazquez and S. Wuchty for discussions; and B. Palsson and S. Schuster for comments on the manuscript. Research at Eötvös University was supported by the Hungarian National Research Grant Foundation (OTKA), and work at the University of Notre Dame and at Northwestern University was supported by the US Department of Energy, the NIH and the NSF.

Competing interests statement The authors declare that they have no competing financial interests.

Correspondence and requests for materials should be addressed to A.-L.B. (alb@nd.edu).

Sortilin is essential for proNGF-induced neuronal cell death

Anders Nykjaer[1,2], Ramee Lee[3], Kenneth K. Teng[3], Pernille Jansen[1,4], Peder Madsen[1], Morten S. Nielsen[1], Christian Jacobsen[1], Marco Kliemannel[5], Elisabeth Schwarz[5], Thomas E. Willnow[2,4], Barbara L. Hempstead[3] & Claus M. Petersen[1]

[1]*Department of Medical Biochemistry, Ole Worms Allé 170, Aarhus University, and* [2]*ReceptIcon Aps, Gustav Wieds vej 10, DK-8000 Aarhus C, Denmark*
[3]*Weill Medical College of Cornell University, New York, New York 10021, USA*
[4]*Max-Delbrück-Center for Molecular Medicine, 13125 Berlin, Germany*
[5]*Institute for Biotechnology, Martin-Luther-Universität, Halle-Wittenberg, 06120 Halle, Germany*

Sortilin[1] (~95 kDa) is a member of the recently discovered family of Vps10p-domain receptors[2,3], and is expressed in a variety of tissues, notably brain, spinal cord and muscle. It acts as a receptor for neurotensin[4,5], but predominates in regions of the nervous system that neither synthesize nor respond to this neuropeptide[6], suggesting that sortilin has additional roles. Sortilin is expressed during embryogenesis[7] in areas where nerve growth factor (NGF) and its precursor, proNGF, have well-characterized effects[6,7]. These neurotrophins can be released by neuronal tissues[8,9], and they regulate neuronal development through cell survival and cell death signalling. NGF regulates cell survival and cell death via binding to two different receptors, TrkA and $p75^{NTR}$ (ref. 10). In contrast, proNGF selectively induces apoptosis through $p75^{NTR}$ but not TrkA[11]. However, not all $p75^{NTR}$-expressing cells respond to proNGF, suggesting that additional membrane proteins are required for the induction of cell death. Here we report that proNGF creates a signalling complex by simultaneously binding to $p75^{NTR}$ and sortilin. Thus sortilin acts as a co-receptor and molecular switch governing the $p75^{NTR}$-mediated pro-apoptotic signal induced by proNGF.

Binding of NGF was examined by surface-plasmon resonance (SPR). As demonstrated in Fig. 1a, sortilin bound mature NGF with moderate affinity (dissociation constant (K_d) ~90 nM). In contrast, the affinity of NGF for $p75^{NTR}$ and TrkA was high (K_d 1–2 nM), in accordance with previous studies in cells[11–13]. As the NGF precursor (proNGF) may escape intracellular processing and be released extracellularly, we next examined binding of proNGF[9,11,14,15]. Whereas lack of processing reduces the affinity of proNGF for $p75^{NTR}$ and TrkA (K_d ~15–20 nM), it results in a much higher affinity (K_d ~5 nM) for sortilin (Fig. 1a). This is surprising because